Journal of Inflammation Research

Dovepress
Taylor & Francis Group

Open Access Full Text Article

ORIGINAL RESEARCH

Cerium Oxide-Loaded Exosomes Derived From Regulatory T Cells Ameliorate Inflammatory Bowel Disease by Scavenging Reactive Oxygen Species and Modulating the Inflammatory Response

Simei Yue[1,*], Lingjiao Gong[1,*], Yulin Tan[1], Xiaodan Zhang[1], Fei Liao[1–3]

[1]Department of Gastroenterology, Renmin Hospital of Wuhan University, Wuhan, Hubei, 430000, People's Republic of China; [2]Wuhan University Shenzhen Research Institute, Shenzhen, Guangdong, 518000, People's Republic of China; [3]Central Laboratory of Renmin Hospital of Wuhan University, Wuhan, Hubei, 430000, People's Republic of China

*These authors contributed equally to this work

Correspondence: Fei Liao, Department of Gastroenterology, Renmin Hospital of Wuhan University, Wuhan, Hubei, 430000, People's Republic of China, Email feiliao@whu.edu.cn

Background: Abnormal immune homeostasis, which leads to the accumulation of reactive oxygen species (ROS) and an inflammatory response, plays a crucial role in accelerating the progression of inflammatory bowel disease (IBD). The lack of targeted therapeutic strategies significantly hampers the efficacy of clinical treatments for IBD. This study presents cerium oxide nanoparticle-loaded regulatory T cell-derived exosomes (exo@nCeO) as innovative anti-inflammatory and antioxidant agents specifically designed to address the effects of immune dysregulation.

Methods: In this work, the morphology and antioxidant properties of nano-cerium oxide were characterized using transmission electron microscopy, as well as hydroxyl radical and 1,1-diphenyl-2-picrylhydrazyl radical assays. Tumor necrosis factor-α and dextran sulfate sodium were employed to establish cellular and animal models of IBD. The impact of exo@nCeO on ROS scavenging and anti-inflammatory activity in intestinal epithelial cells was assessed using dihydroethidium and 2,7-dichlorodihydrofluorescein staining, Western blotting, and apoptosis flow cytometry analysis. Hematoxylin and eosin staining, along with immunohistochemistry and immunofluorescence staining, were utilized to evaluate intestinal epithelial inflammation and ROS levels in the IBD mouse model.

Results: The findings demonstrate that exo@nCeO possesses augmented anti-inflammatory properties and ROS scavenging abilities in intestinal epithelial cells. In murine models of IBD, exo@nCeO effectively maintained the integrity of the intestinal epithelial barrier and impeded the progression of IBD.

Conclusion: This study introduces a novel therapeutic approach for IBD and underscores a potential strategy for addressing diseases associated with inflammation and oxidative stress.

Keywords: inflammatory bowel disease, regulatory T cells, exosomes, cerium oxide

Introduction

Inflammatory bowel disease (IBD) is a chronic inflammatory disorder characterized by diarrhea, bloody stools, inflammation of the gastrointestinal tract, and an impaired immune system.[1] A range of clinical treatments is available for IBD, including sulfasalazine, 5-aminosalicylic acid, biologics, and immunomodulators.[2] However, existing treatments for IBD are associated with adverse effects when use long-term, including immunosuppression, hepatotoxicity and nephrotoxicity.[3] Consequently, there is a serious need for the development of novel therapeutic agents for IBD.

Received: 23 October 2024
Accepted: 14 March 2025
Published: 25 March 2025

Graphical Abstract

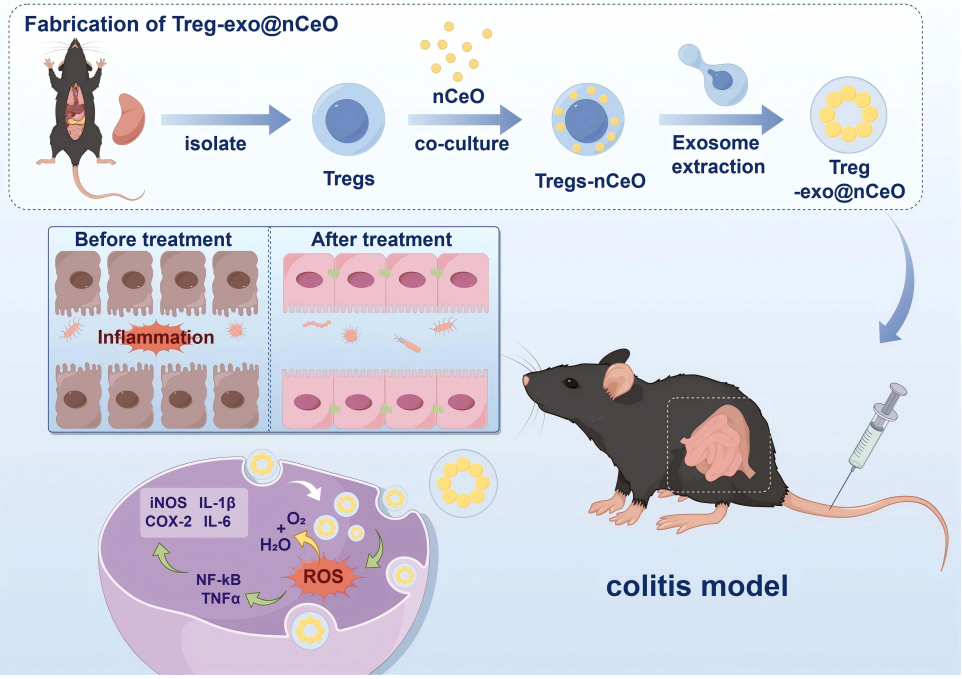

Regulatory T cells (Tregs), a subset of CD4+ T helper cells, have been demonstrated to play a crucial role in IBD by exerting anti-inflammatory effects within the intestinal.[4] A reduced presence of Tregs has been observed in IBD mouse models, which correlates with exacerbated intestinal inflammatory responses.[5] The induction of CD4+ T cell differentiation into Tregs in vivo has demonstrated promising outcomes in ameliorating clinical symptoms of IBD.[6] Recently, exosomes, the nano-sized (30–150 nm) vesicles released from cells, have been shown to be the critical mediator in the regulation of immune homeostasis by Tregs.[7] In our previous research, we established the therapeutic efficacy of Treg-derived exosomes in the context of IBD, prompting us to further explore the development of a Treg-exosome-based therapeutic strategy for this condition.[8]

Excessive reactive oxygen species (ROS) are regarded as central factors exacerbating IBD by increasing intestinal membrane permeability and triggering deleterious immune responses within the intestine.[9] The ROS scavenging was inhibited in IBD patients, causing inflammatory response and damage to the intestinal mucosa.[10] Agents with the ability to scavenge ROS have shown remarkable therapeutic effects in IBD. Cerium oxide nanoparticles (nCeO) are potent nanozymes exhibiting catalase and superoxide dismutase mimetic activities, enabling them to scavenge various ROS, including hydrogen peroxide and hydroxyl radicals.[11] In comparison to other reducing agents, nCeO offers several distinct advantages, including high efficiency, versatility, stability, cost-effectiveness, and minimal immunogenicity. These properties have facilitated its widespread application in various ROS-related diseases.[12] Nevertheless, the elevated scavenging rate and reduced internalization of small-sized nCeO present obstacles for their clinical application.[13]

Furthermore, the intricate environment of the gastrointestinal tract may impede the effective targeting of inflammatory regions by nCeO following oral administration, potentially resulting in suboptimal therapeutic outcomes. Synthetic drug carriers have garnered significant attention for their capacity to enhance the pharmacokinetics and pharmacodynamics of conventional drugs while mitigating toxicity and side effects. Among these carriers, lipid nanoparticles (LNPs) exhibit promise for drug delivery; however, they encounter challenges such as low bioavailability, difficulty in clearance from the bloodstream, and immune reactions,[14] which necessitate further investigation to optimize their clinical applications.

Exosomes, which are structurally similar to liposomes, possess certain advantages that render them an ideal vehicle for drug delivery.[15] Their favorable interaction with cell membranes, rapid internalization, and excellent biocompatibility demonstrate significant potential for targeted therapy and bioengineering applications.[16]

In this study, we propose an innovative approach that combines nCeO with exosomes derived from regulatory T cells. This combination is designed to address IBD by reducing intracellular ROS levels and modulating the inflammatory response.

Materials and Methods

Synthesis and Characterization of Cerium Oxide Nanoparticles

Cerium nitrate hexahydrate (4 mmol, 10294–41-4, Aladdin, Shanghai, China) and oleylamine (12 mmol, 112–90-3, Aladdin, Shanghai, China) were dissolved in 20 g of 1-octadecene (112–88-9, Aladdin, Shanghai, China). The mixture was heated under a vacuum at 80 °C for 1 h and heated at 260 °C for 2 h in an argon atmosphere. The resulting solution was cooled to room temperature and washed several times with cyclohexane and anhydrous ethanol using centrifugation (15,000 rpm for 20 min). The resulting nCeO were redispersed in chloroform. For water dispersion and fluorescent labeling, nCeO was encapsulated with $mPEG_{2k}$-DSPE or Cy5-PEG_{2k}-DSPE. To achieve this, 30 mg of $mPEG_{2k}$-DSPE (supplement with 5 mg Cy5-PEG_{2k}-DSPE for fluorescent labeling) were dissolved in 5 mL of nCeO/chloroform (2 mg/mL). The mixture was stirred at room temperature for 4 h and the chloroform was removed from the sample using a rotary evaporator. Next, 10 mL of ultrapure water was added to the sample and sonicated for 30 min. nCeO was purified by filtration, ultracentrifugation and dialysis. nCeO concentrations were assessed by Inductively Coupled Plasma-Atomic Emission Spectroscopy (ICP-OES, Agilent 5110, Agilent, US). Morphology and elemental distribution of nCeO were detected by the transmission electron microscopy (TEM, FEI Tecnai G2 spirit, Thermo) and the energy dispersive spectrometer (EDS).

Antioxidant Capacity Assay

Different concentrations of nCeO were added into 30% hydrogen peroxide (H112519, Aladdin, Shanghai, China) and catalase activity was evaluated by measuring the level of dissolved oxygen with a portable dissolved oxygen meter every 10 min. The free radical scavenging ability was assessed by Hydroxyl Free Radical assay kit (A018-1-1, Nanjing jiancheng, Nanjing, China) and 2.2-Diphenyl-1-picrylhydrazyl (DPPH) Free Radical Scavenging Capacity Assay Kit (A153-1-1, Nanjing jiancheng, Nanjing, China) according to the manufacturer's protocol.

Isolation and Identification of Treg Cells

CD4+CD25+ Tregs were isolated using the mini-MACS immunomagnetic separation system (130–091-041, Miltenyi Biotec, Germany) according to the manufacturer's protocol. 1×10^6 Tregs were collected and stained with phycoerythrin (PE) monoclonal antibodies against mouse CD25 (E-AB-F1102D, Elabscience, China) and fluorescein isothiocyanate (FITC) conjugated monoclonal antibodies against mouse CD4 (E-AB-F1097C, Elabscience, China) for 30 min, followed by data collection on a flow cytometer (Beckman Coulter, USA). For cytotoxicity assay, Treg cells were cultured with different concentrations of nCeO and stained with trypan blue.

Extraction and Identification of Treg Cells-Exosomes

The exosomes (exo) were isolated by using the Hieff® Quick exosome isolation kit Plus for Cell Culture Media (41201ES20, Yeason, Shanghai, China) according to the manufacturer's instructions. For the cerium oxide nanoparticle-loaded regulatory T cell-derived exosomes (exo@nCeO), Tregs were pretreated with 50 μg/mL nCeO for 24 h. The morphology of exosomes was characterized using TEM, nanoparticle tracking analysis (NTA, NanoSight NS300, Malvern), and Western blot. For exosomes labeling, exosomes were stained with 1 μM Dio dye (G1704, Servicebio, Wuhan, China) for 30 minutes at 37 °C. Extracted exosomes were dissolved in phosphate buffered saline (PBS) and purified by an ultrafiltration tube (Millipore, MW=3KDa). The purified exo@nCeO was evaluated for Ce concentration by ICP-OES to calculate the encapsulation rate according to the following formula:

$$\%\,\text{Encapsulation} = 100\% \times \frac{\text{encapsulated nCeO in exosome}}{\text{total mass of added nCeO}}$$

Cellular Antioxidant Capacity Assay

NCM460 were purchased from the Guangzhou Cellcook Biotech Co.,Ltd (China) and seeded in six-well. After conglutination, the cells were intervened with TNF-α (50 ng/mL, RP02081, Abclonal, China), 1×10^8 particles/mL exo and exo@nCeO for 24 h. Next, the complete medium was removed and incubated with 10 μM 2′,7′-Dichlorodihydrofluorescein diacetate (DCFH-DA, S0033S, Beyotime, Shanghai, China) or 10 μM Dihydroethidium (DHE, 50102ES02, Yeason, Shanghai, China) dissolved in serum-free medium for 30 min. After washing with PBS, the mean fluorescence intensity was captured using an inverted fluorescence microscope and flow cytometer.

Western Blots

Total proteins of NCM460 were isolated using RIPA buffer (G2002, Servicebio, China) supplemented with 1 mm Phenylmethanesulfonyl fluoride (PMSF, G2008, Servicebio, China) and protease inhibitors cocktail (G2006, Servicebio, China). The protein was separated by 12% sodium dodecyl sulfate-polyacrylamide gel (G2044, Servicebio, China) electrophoresis and transferred to a polyvinylidene fluoride (PVDF, Baseniaobio) membrane. The PVDF membrane was incubated with the primary anti-Calnexin (1:1000, A4846, Abclonal, China), anti-Tsg101 (1:1000, A2216, Abclonal, China), anti-CD63 (1:2000, A19023, Abclonal, China), anti-GAPDH (1:3000, GB11002, Servicebio, China), anti-iNOS (1:1000, A14031, Abclonal, China), anti-COX2 (1:1000, A1253, Abclonal, China), anti-IL-1β (1:1000, A16288, Abclonal, China), anti-IL-6 (1:1000, A22222, Abclonal, China), anti-BAX (1:1000, A19684, Abclonal, China) and anti-BCL-2 (1:1000, A19693, Abclonal, China) overnight at 4°C. After washing three times with phosphate buffered saline tween 20 (PBST), the PVDF membrane was incubated with the secondary antibody (1:5000, GB23303, Servicebio, China) at room temperature for 2 h. Protein bands were visualized using ECL luminescent liquid (SQ101, Epizyme Biotech, USA) on ChemiDoc Touch (Bio-Rad, CA, USA). Semi-quantitative analysis of the images was performed using ImageJ software (Version: 1.8.0).

Real-Time Quantitative PCR (RT-qPCR)

NCM460 cells were inoculated at a density of 3×10^5 cells per well in a 6-well plate and incubate for 24 h. After stimulation with TNF-α (50 ng/mL, RP02081, Abclonal, China) for 2 h, the treatment group was supplemented with 1×10^8 particles/mL exo@nCeO. Total RNA was extracted using animal RNA isolation kit (R0026, Beyotime, China), and reverse transcribe by SweScript RT II Enzyme Mix (G3330, Servicebio, China) according to the manufacturer's protocol. Quantitative analysis was performed by LightCycler 480 Software (Roche, Switzerland) and Universal SYBR Green Fast qPCR Mix Kit (G3320, Servicebio, China). The primer sequences used in this study are as follows.

β-ACTIN: forward 5′-CACCCAGCACAATGAAGATCAAGAT-3′,
reverse 5′-CCAGTTTTTAAATCCTGAGTCAAGC-3′;
CXCL2: forward 5′-CTGCAGGGAATTCACCTCAA-3′,
reverse 5′-CAAGCTTTCTGCCCATTCTT-3′;
CXCL8: forward 5′-GAAGGTGCAGTTTTGCCAAG-3′,
reverse 5′-GGGTCCAGACAGAGCTCTCT-3′;
CXCL10: forward 5′-GCCATTCTGATTTGCTGCCT-3′,
reverse 5′-GACAAAATTGGCTTGCAGGA-3′;
CYP3A4: forward 5′-CCCACACCTCTGCCTTTTTT-3′,
reverse 5′-CCTCCGGTTTGTGAAGACAG-3′;
CYP3A5: forward 5′-ATCCCGACGTGATCAGAACA-3′,
reverse 5′-TTGGAGACAGCAATGACCGT-3′;
CYP2B6: forward 5′-ACCCATTCTTCCGGGGATAT-3′,
reverse 5′-TTGGATTTCCGAAGCTCCTC-3′.

Apoptosis Flow Cytometry

Apoptotic cells were stained by Annexin V-FITC/PI Apoptosis Kit (E-CK-A211, Elabscience, China) according to the manufacturer's protocol and analyzed by flow cytometry. Data were collected on a flow cytometer (CytoFlex, Beckman Coulter, USA).

RNA-Seq

mRNA enrichment was conducted on total RNA utilizing oligo (dT)-attached magnetic beads. The mRNA enriched with poly (A) tails underwent fragmentation via a fragmentation buffer, followed by reverse transcription using random hexamer primers (N6) to synthesize double-stranded complementary DNA. Subsequently, the synthesized double-stranded DNA underwent end-repair and 5′-phosphorylation, with the addition of an "A" overhang at the 3′-end to create a blunt end. This was followed by the ligation of an adapter with a "T" overhang at the 3′-end. The ligation products were then subjected to amplification through PCR using specific primers. The constructed libraries were quality controlled and sequenced after passing the quality-control. Sequencing was performed on the DNBSEQ platform using PE150 (read length).

Bioinformatics Analysis

Genes differentially expressed between TNF-α and TNF-α+exo@nCeO were manually annotated for protein function using Gene Ontology (GO) and Kyoto Encyclopedia of Genes and Genomes (KEGG) enrichment analyses. The clusterProfiler package in R was used for functional annotation and visualization. Gene set enrichment analysis (GSEA) was also performed using the GSEA software. The Search Tool for the Retrieval of Interacting Genes (version 11.4) database was used to construct a PPI network and the cytoHubba plugin was utilized to screen for hub genes.

Animal Experimentation

The animal study protocol was conducted in compliance with the National Research Council's Guide for the Care and Use of Laboratory Animals and approved by the Institutional Animal Care and Use Committee of Renmin Hospital of Wuhan University (Approval No: 20211106). Six-week-old male C57BL/6 mice were procured from SiPeiFu Biotechnology Co., Ltd. (Beijing, China) and maintained in a controlled barrier environment at 25 °C. To induce an acute colitis model, the mice were administered 3% dextran sulfate sodium (DSS) in their drinking water for a duration of eight consecutive days. During this treatment period, the mice were randomly allocated into five distinct groups: negative control group (sterile water), DSS group (3% DSS), DSS+nCeO treatment group (3% DSS+20 μg nCeO), DSS +exo treatment group (3% DSS+1×10^9 particles exo), DSS+exo@nCeO treatment group (3% DSS+1×10^9 particles exo@nCeO). Commencing one day post-DSS treatment, intravenous injections of the respective treatments were administered every two days. Throughout the eight-day period, the mice were meticulously monitored for weight loss, stool consistency (0: hard, 2: soft, 4: diarrhea), and rectal bleeding (0: negative, 2: positive, 4: macroscopic)[17] employing a fecal occult blood test (60403ES60, Yeason, Shanghai, China). These observations facilitated the calculation of the disease activity index (DAI), thereby providing a comprehensive evaluation of the mice's condition.

On the eighth day following DSS treatment, the mice were humanely euthanized, and isolated the colon for length measurement. Colon was fixed in 4% paraformaldehyde for 24 h and embedded in paraffin. The tissues were then cut into 5 μm sections for histological staining or immunohistochemical analysis. The remaining colon was frozen in liquid nitrogen for the ROS assay.

For biosafety assessment, mice were divided into NC group and exo@nCeO group (n=6), and the latter was given the same frequency and concentration of exo@nCeO intervention. The heart, liver, lung and kidney was fixed in 4% paraformaldehyde for 24 h and embedded in paraffin for subsequent analysis. Furthermore, alkaline phosphatases (ALP), alanine aminotransferase (ALT), aspartate aminotransferase (AST), creatinine (CREA) and urea nitrogen (BUN) through automatic biochemical analyzer (Chemray 800, Shenzhen RADu Life Technology, China).

Histological Experiments

The embedded tissue was cut into 5 μm sections for Hematoxylin-Eosin (HE) staining, immunohistochemistry, immunofluorescence and ROS staining. For immunohistochemistry staining, the sections were blocked with 3% BSA (A8010, Solarbio, China) at room temperature for 30 minutes. Then, sections were incubated with primary antibody anti-iNOS (1:200, A14031, Abclonal, China), anti-COX2 (1:200, A1253, Abclonal, China), anti-IL-6 (1:200, A22222, Abclonal, China) and anti-IL-1β (1:200, A16288, Abclonal, China),overnight at 4 °C. After washing with PBST, sections were covered with fluorescently labeled secondary antibody or HRP-conjugated secondary antibody at room temperature for 1 h. Finally, an upright optical microscope (BX53, OLYMPUS, Japan) was used to capture images for analysis of the protein expression at the intestinal mucosa. For ROS staining, frozen sections were stained by DHE according to the manufacturer's protocol.

Near-Infrared Fluorescence (NIRF) Imaging

According to the experimental design above, same concentration of nCeO and exo@nCeO labelled with Cy5 were administered into the mice treated with DSS. After sacrifice, organs, including the heart, liver, spleen, kidney, and colon tissues, were collected for ex vivo imaging by using IVIS Spectrum (PERKINELMER, USA).

Statistical Analysis

In this study, all data are presented as mean ± standard deviation and were analyzed using one-way analysis of variance (ANOVA) followed by Dunnett' test (compare multiple experimental groups with one control group) or Tukey's test (compare the different groups with each other) were administrated with Prism software (Version: 8.0). A p-value of less than 0.05 was considered indicative of statistical significance.

Results

Fabrication and Characterization of Treg-exo@nCeO

Firstly, the nCeO was synthesized by the thermal decomposition method. TEM and EDS analyses confirmed a uniform size and a cerium-to-oxygen atomic ratio of 1:2 (Figure 1A and B). Furthermore, the nCeO were stable in an aqueous solution at room temperature for one week (Figure 1C). To assess the catalytic activity of the nCeO, a series of enzyme mimicking activities were conducted. Specifically, hydrogen peroxide, hydroxyl radical, and DPPH scavenging assays were employed to evaluate the overall antioxidant capacity of nCeO. The finding indicated that nCeO exhibited significant antioxidant capacity with a dose-dependent manner (Figure 1D–F).

Additionally, an immunomagnetic separation system was utilized to isolate Tregs from the spleens of mice. Flow cytometric analysis demonstrated a purity of 88.17% for CD4+CD25+ Tregs (Figure 1G). To investigate the impact of nCeO on the cytotoxicity of Tregs, we performed trypan blue staining to quantify the proportion of viable cells. As shown in Figure 1H and I, nCeO was internalized by Tregs and demonstrated safety at concentrations below 50 μg/mL, which was the concentration employed in subsequent experiments.

The extracted exosomes were characterized by TEM analysis, Western blot and NTA, revealing cup-shaped microparticles with an average diameter of approximately 100 nm, expressing positive markers for Tsg101 and CD63. Notably, nCeO was detected within the exosomes, and its presence did not alter the exosome size (Figure 1J–L, $p > 0.05$). Among them, the encapsulation rate of cerium oxide nanoparticles in exosomes was 34.85±3.77% and drug loading was 6.67 ± 0.85μg/10^8 particals. The exo@nCeO was then labelled with Dio and co-cultured with NCM460 cells. The results showed co-localization of red and green fluorescence within the NCM460 cells, indicating the successful preparation of exo@nCeO and its uptake by these cells (Figure 1M). Moreover, trypan blue staining showed that both exo and exo@nCeO had no effect on the activity of NCM460 cells (Figure S1).

Treg-exo@nCeO Inhibited Intestinal Epithelial Cell Inflammation and Apoptosis

Given the ROS scavenging function of nCeO, we investigated the effect of exo@nCeO against oxidative damage in NCM460 cells. In comparison to TNF-α-induced ROS accumulation, intracellular ROS levels were significantly diminished in both the nCeO and exo@nCeO groups, especially in the latter (Figure 2A–F, $p < 0.05$). Next, the impact

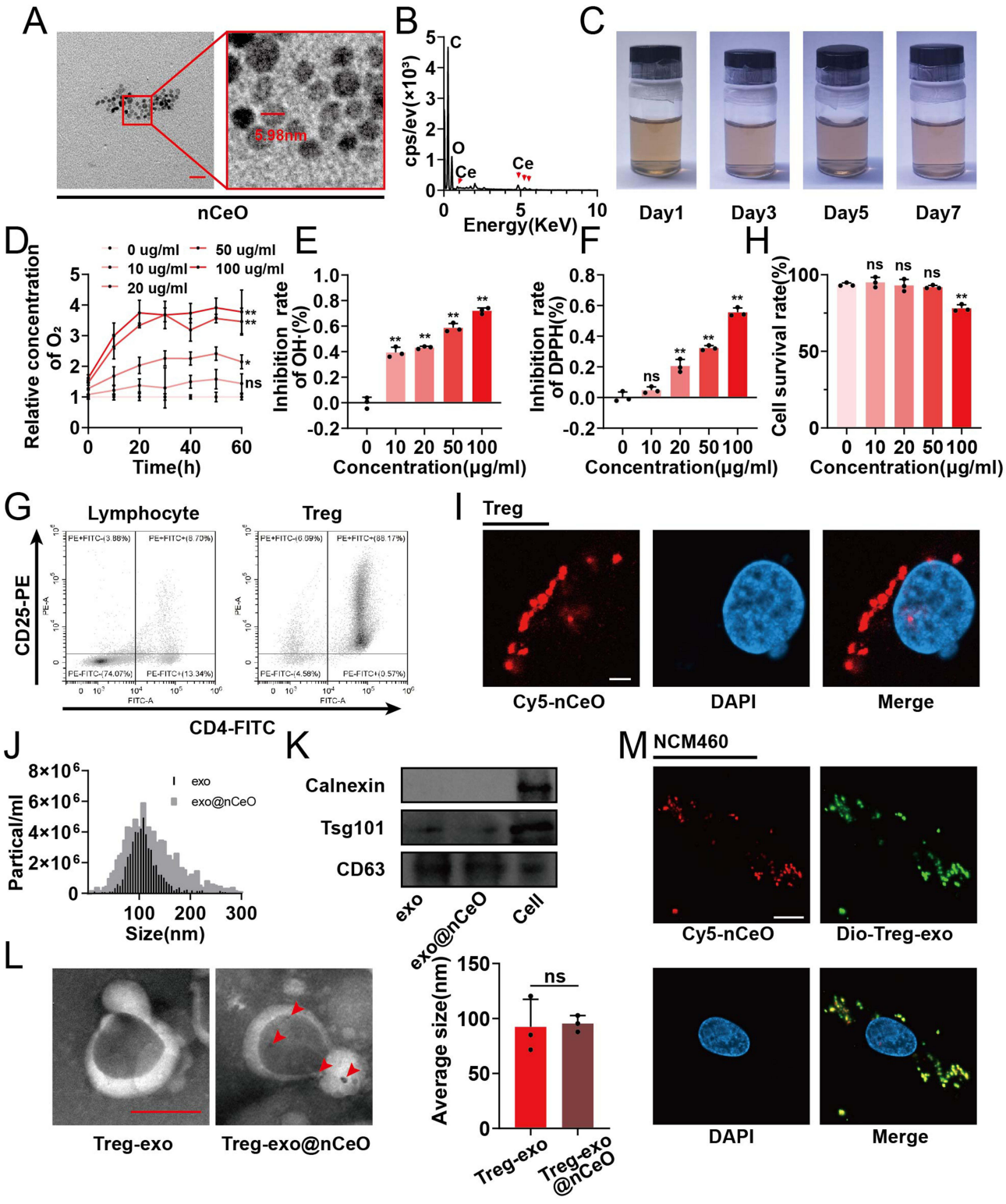

Figure 1 Synthesis and characterization of Treg-exo@nCeO. (**A**) TEM images of nCeO, scale bars: 10 nm. (**B**) EDS spectrum of nCeO. (**C**) Appearance images of nCeO. (**D–F**) hydrogen peroxide and free radical scavenging assay, n=3; *p < 0.05 vs 0 μg/mL, **p < 0.01 vs 0 μg/mL, ns, no significance vs 0 μg/mL. (**G**) Flow chart of the isolation of CD4+CD25+ T cells. (**H**) Relative proportion of living cells, n=3; **p < 0.01 vs 0 μg/mL, ns, no significance vs 0 μg/mL. (**I**) Uptaken Cy5-labeled nCeO and fluorescence imaging, scale bars: 2 μm. (**J**) NTA of exo and exo@nCeO. (**K**) Western blot assay of the expression of Calnexin, Tsg101 and CD63 in Tregs and exo. (**L**) TEM images and average size of exo and exo@nCeO, n=3, scale bars: 100 nm. (**M**) Uptaken Dio-exo@Cy5-nCeO and fluorescence imaging, scale bars: 5 μm.

https://doi.org/10.2147/JIR.S502388

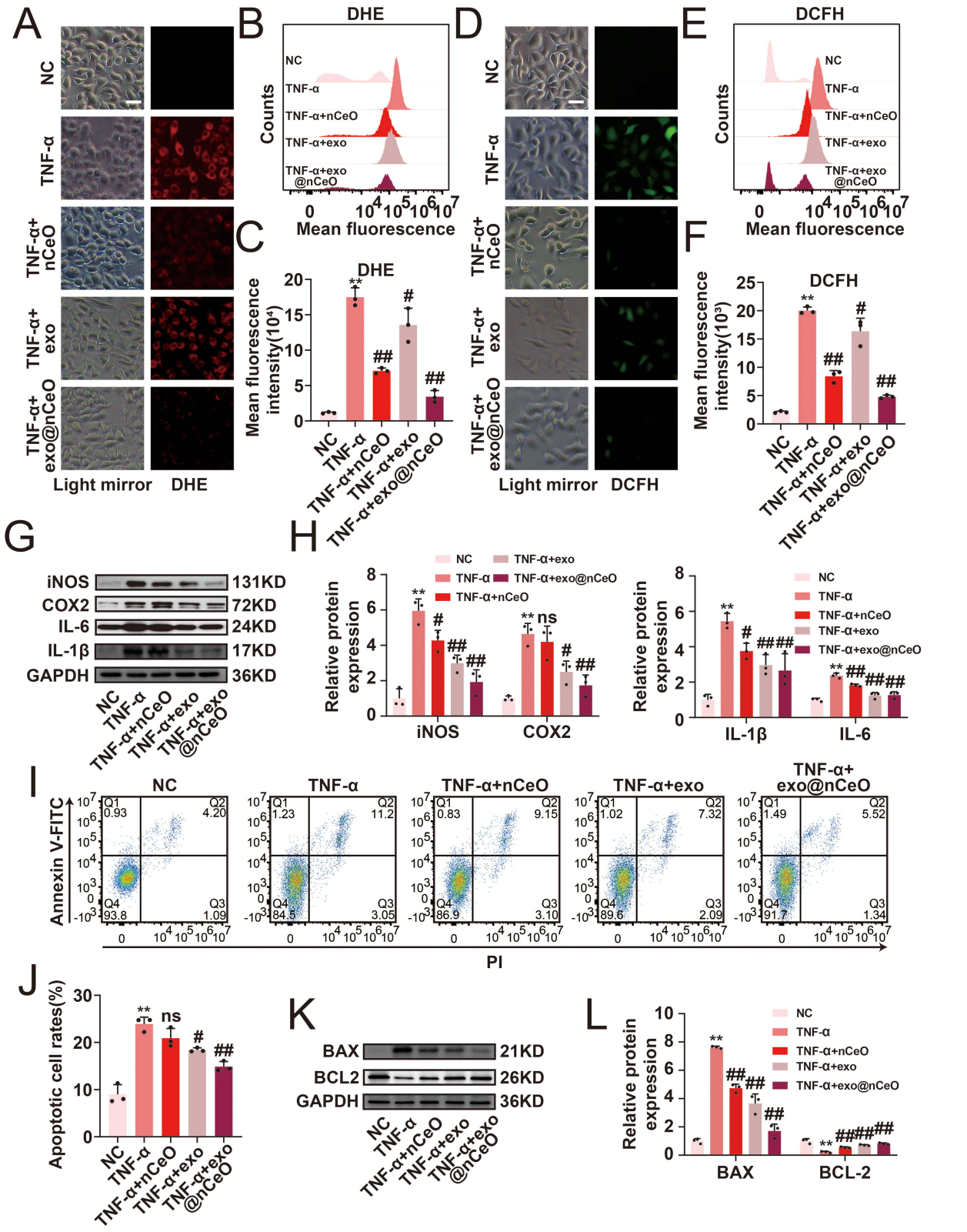

Figure 2 exo@nCeO inhibited intestinal epithelial cell inflammation and apoptosis. (**A** and **D**) Representative fluorescence images of DCFH and DHE probes, scale bars: 10 μm. (**B**, **C**, **E** and **F**) Flow chart of the DCFH and DHE probes, and mean fluorescence intensity. (**G**, **H**, **K** and **L**) Western blot assay and semi-quantitative analysis of the expression of iNOS, COX2, IL-1β, IL-6, BAX and BCL-2 in different group. (**I** and **J**) Flow chart of the apoptotic cells and apoptotic cells rates. n=3, $^{**}p < 0.01$ vs NC, $^{\#}p < 0.05$ vs TNF-α, $^{\#\#}p < 0.01$ vs TNF-α, no significance vs TNF-α.

https://doi.org/10.2147/JIR.S502388

of exo@nCeO on TNF-α-induced inflammatory response was assessed. Western blot analyses confirmed that exo, nCeO and exo@nCeO reduced the expression of iNOS, COX2, IL-1β and IL-6, with exo@nCeO demonstrating the most substantial effects (Figure 2G and H, $p < 0.05$).

The increased apoptosis of epithelial cells in IBD compromises the integrity of the mucosal epithelial barrier and accelerates disease progression.[18] Thus, we evaluated the role of exo@nCeO in TNF-α-induced apoptosis. Flow cytometry experiments showed that the proportion of apoptotic NCM460 was decreased by exo@nCeO compared to the TNF-α group (Figure 2I and J, $p < 0.05$). Correspondingly, the expression of the pro-apoptotic factor BAX was downregulated and that of the anti-apoptotic factor BCL2 was increased in exo@nCeO-treated NCM460 cells (Figure 2K and L, $p < 0.05$).

Collectively, these findings indicate that exo@nCeO confers protection to cells against inflammation and apoptosis.

Transcriptomic Characterization of Treg-exo@nCeO Treatment

To systematically evaluate the role of exo@nCeO in the pathogenesis of IBD at the transcriptomic level, we performed RNA-seq analysis on NCM460 cells subjected to exo@nCeO treatment (Table S1). The transcriptomic analysis revealed 352 differentially expressed genes (DEGs) (fold change > 2, p.adj < 0.05) in the TNF-α+exo@nCeO group when comparing the TNF-α group (106 upregulated and 246 downregulated) (Figure 3A and B, Table S2). Functional annotation results showed that up-regulated and down-regulated DEGs were enriched in xenobiotic metabolism and inflammatory pathways, respectively (Figure 3C–E) Next, GSEA was employed to further investigate the impact of exo@nCeO on TNF-α-associated inflammatory processes. The analysis revealed significant differences (FDR < 0.05, nominal $p < 0.05$) in the enrichment of pathways related to the inflammatory response and TNF signaling via the NF-κB pathway (Figure 3F and G). Finally, we constructed the PPI network and screened hub genes within the up-regulated and down-regulated DEGs. The results indicated that the hub down-regulated DEGs were predominantly associated with inflammatory cytokines such as TNF, IL1B, IL1A and IL6. Meanwhile, the hub up-regulated DEGs were primarily linked to drug-metabolizing enzymes including *CYP3A4, CYP3A5, CYP2B6* and *CYP26A1* (Figure 3H and I). The top three up-regulated hub-gene and three down-regulated hub-gene were validated by RT-qPCR. The results confirmed that exo@nCeO down-regulated the expression of *CXCL10, CXCL8* and *CXCL2*, while up-regulated the expression of *CYP3A5, CYP3A4*, and *CYP2B6*, which is consisted with the RNA-sequencing results (Figure S2). Overall, these results suggest that exo@nCeO has the potential to attenuate the inflammatory response triggered by TNF-α while simultaneously enhancing the drug metabolism process.

Therapeutic Effect of Treg-exo@nCeO in a DSS-Induced IBD Mouse Model

To evaluate the effect of exo@nCeO on colitis, mice were treated with DSS to establish the IBD model (Figure 4A). We found that exo@nCeO significantly increased the colon length compared to the DSS group (Figure 4B, $p < 0.05$). Meanwhile, body weight and Disease Activity Index (DAI) scores were also improved in the DSS+exo@nCeO group (Figure 4C and D, $p < 0.05$). The results of HE staining and histological score in colon tissue also suggested a protective effect of exo@nCeO against colitis (Figure 4E and F, $p < 0.05$). Furthermore, both the DSS+nCeO and DSS+exo groups exhibited comparatively milder therapeutic effects than the DSS+exo@nCeO group.

Next, we conducted an analysis of the inflammatory response levels in colon tissue using immunohistochemical staining. The pro-inflammatory factors iNOS, COX2, IL-1β and IL-6 were increased in the colon of DSS-induced colitis (Figure 4G). However, various treatment groups demonstrated the potential to modulate the expression of these pro-inflammatory factors, with exo@nCeO significantly inhibiting the expression of iNOS, COX2, IL-1β, and IL-6. Damage to the intestinal barriers constitutes a significant characteristic of DSS-induced colitis.[19] Accordingly, DHE and immunofluorescence staining were used to measure the concentration of ROS and the integrity of the intestinal epithelial barrier, respectively. The results revealed that DSS exposure led to elevated ROS levels and a reduction in the expression of intestinal barrier related protein ZO-1 and Occludin. Conversely, treatment with exo@nCeO markedly decreased ROS concentrations and enhanced the expression of ZO-1 and Occludin (Figure 4H–K, $p < 0.05$).

In terms of distribution, we found that nCeO and exo@nCeO remained enriched in the colon at 48h post-injection, while the fluorescence intensity of the latter was slightly higher than that of the former, suggesting that exosome encapsulation of nCeO may have a facilitating effect on recruitment to inflammatory regions (Figure S3A and B). Some

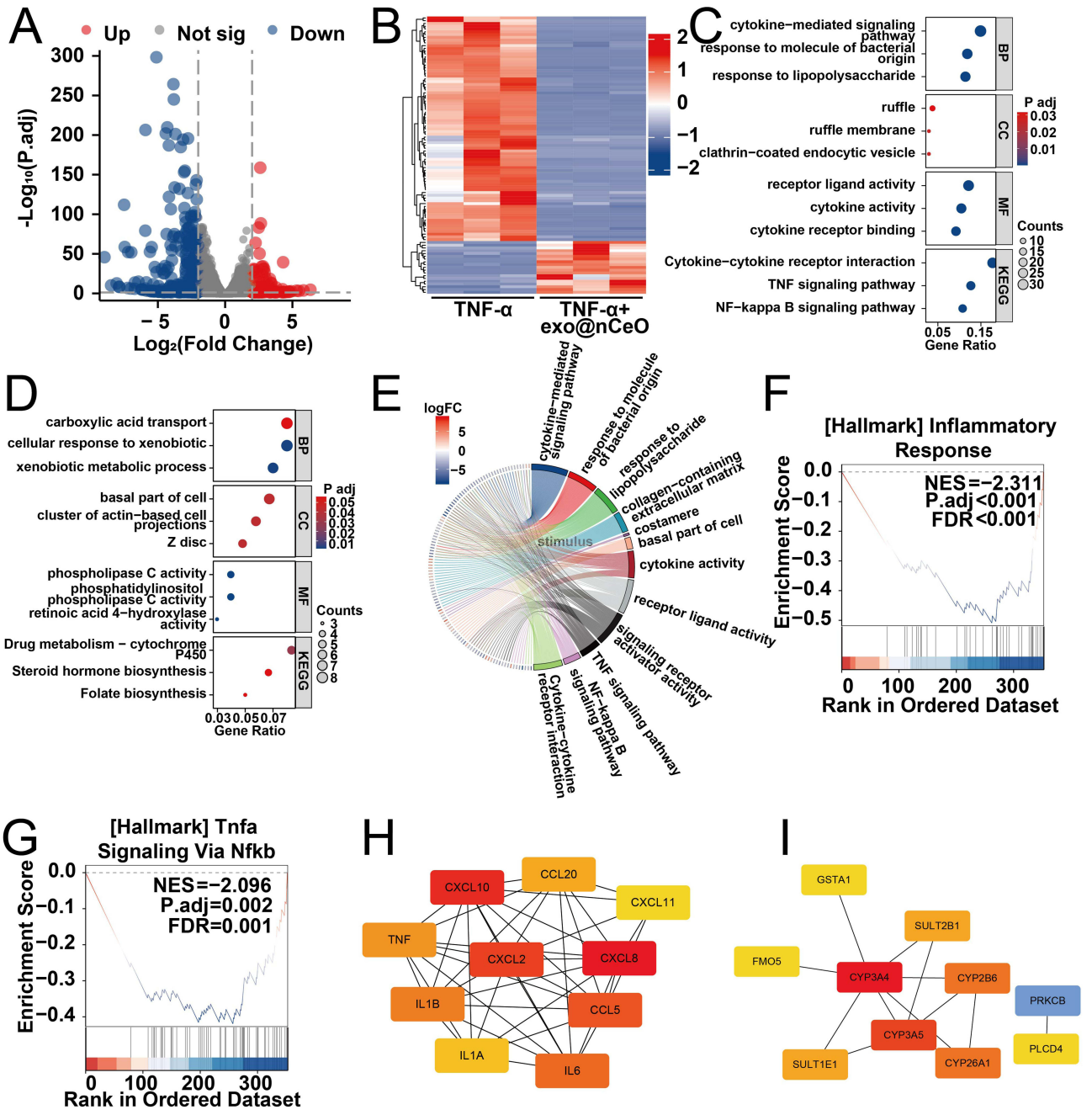

Figure 3 Transcriptomic characterization of Treg-exo@nCeO treatment. (**A** and **B**) Volcano plots and heatmap of DEGs. (**C** and **D**) Bubble graphs of GO and KEGG pathway enrich in downregulated and upregulated DEGs. (**E**) Chord graph of functional annotation analysis. (**F** and **G**) GSEA analysis of DEGs. (**H** and **I**) PPI networks of downregulated and upregulated DEGs.

fluorescence signals were also observed in the kidney and liver, suggesting that the drug might be metabolised through the liver and kidney.

To evaluate the biosafety of exo@nCeO in vivo, we performed the haemolysis assay to evaluate the hemocompatibility of exo@nCeO. After treatment with exo@nCeO (10^2–10^9 particles/mL), haemolysis rates were less than 5% at all concentrations, indicating that exo@nCeO is haemocompatible (Figure S3C). Next, we injected healthy mice with exo@nCeO in the tail vein at the same concentration and frequency, and then examined the changes in major organs and blood in vivo. HE results showed that no significant tissue necrosis was observed in the heart, liver, lungs and kidneys (Figure S3D). Furthermore, as shown in Figure S3E, blood biochemicals such as ALT, AST, and BUN were not

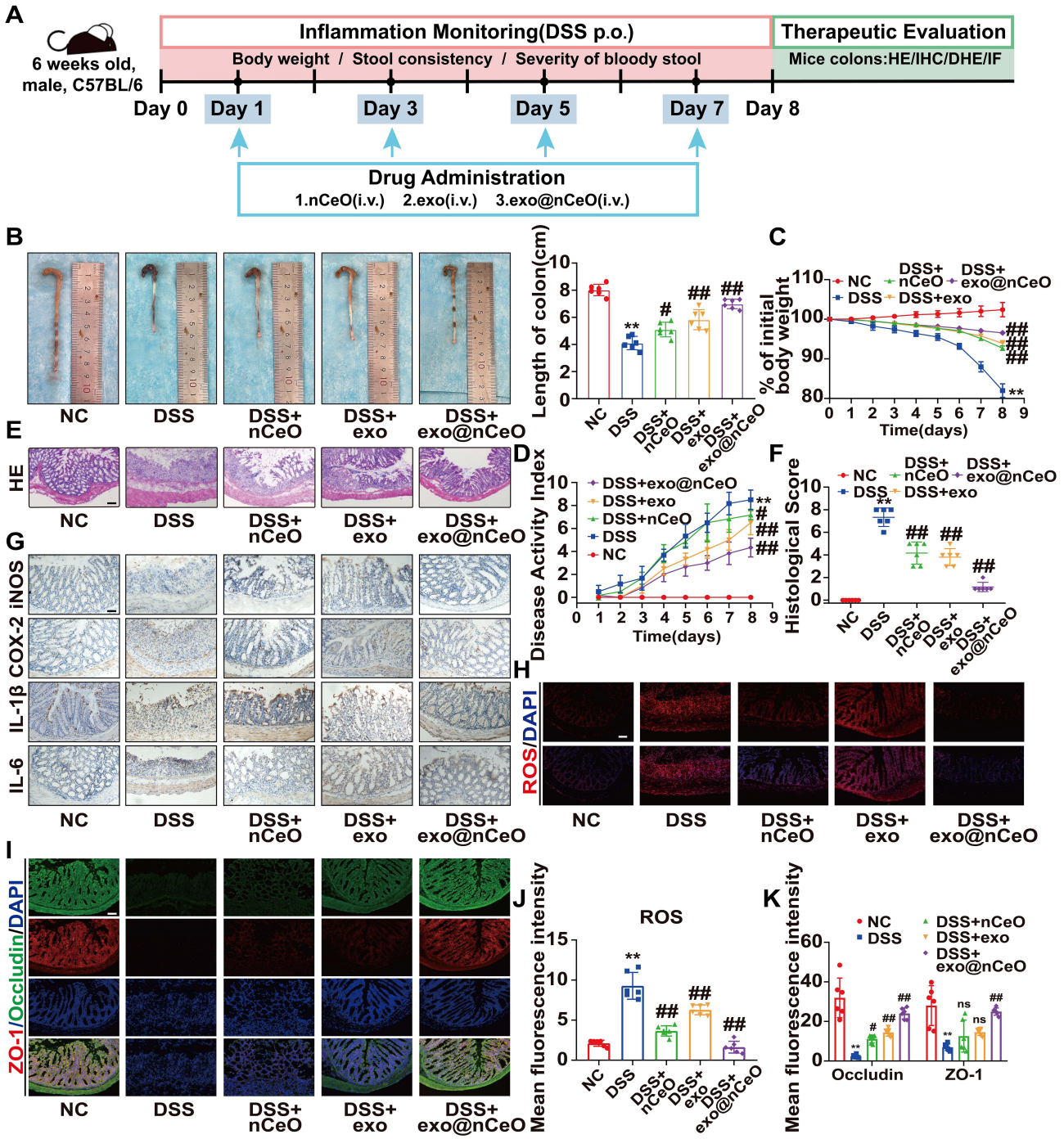

Figure 4 Therapeutic effect of Treg-exo@nCeO in a DSS-induced IBD mouse model. (**A**) Flowchart of animal experiments. (**B**) Representative photographs and quantitative analysis of mice colons in different treatment groups. (**C**) The body weight of mice. (**D**) DAI in each group. (**E** and **F**) HE stained images and histological score after different treatments, scale bars: 100 μm. (**G**) Representative images of IHC staining of iNOS, COX2, IL-1β and IL-6, scale bars: 100 μm. (**H** and **J**) DHE staining and mean fluorescence intensity in each group, scale bars: 100 μm. (**I** and **K**) Immunofluorescence staining and mean fluorescence intensity of ZO-1 and Occludin, scale bars: 100 μm. n=6, $^{**}p < 0.01$ vs NC, $^{\#}p < 0.05$ vs DSS, $^{\#\#}p < 0.01$ vs DSS, ns, no significance vs DSS.

statistically different between NC and exo@nCeO. Together, these data support the biosafety of exo@nCeO in potential biomedical applications.

The aforementioned findings suggest that exo@nCeO mitigated the progression of colitis by suppressing oxidative stress and inflammatory responses, as well as enhancing the intestinal permeability compromised by colitis.

https://doi.org/10.2147/JIR.S502388

Discussion

Intestinal immune homeostasis is crucial in the pathogenesis of IBD.[20] Disruption of immune homeostasis leads to aberrant inflammatory responses and the accumulation of ROS, which are believed to contribute to tissue damage.[21] Therefore, targeting immune regulation and ROS clearance is essential in the management of IBD. In this work, we devised an innovative approach by integrating exosomes derived from Tregs with nCeO to simultaneously address immune dysregulation and oxidative stress. Initially, we successfully synthesized exo@nCeO and demonstrated its anti-inflammatory and antioxidant properties through both in vitro and in vivo experiments. Additionally, our RNA sequencing analysis indicated that exo@nCeO effectively attenuates the progression of IBD by inhibiting the NF-κB signaling pathway. This study not only proposes a promising novel strategy for IBD treatment but also highlights the substantial potential of integrating nCeO with exosomes for therapeutic applications.

Tregs, a subset of CD4+ T cells, are characterized by their immunosuppressive functions.[22] Notably, a marked decrease in the Treg population has been documented in the peripheral blood of mice with experimentally induced colitis.[23] The promotion of differentiation of naive CD4+ T cells into Tregs by metabolites can alleviate IBD in mice, indicating the critical role of Tregs in the progression of IBD.[24] Recent studies have shown that Tregs can mediate immunomodulatory effects through exosomes, an approach noted for its minimal immune response, safety, and high efficacy. This has prompted further investigation into their potential role in IBD. Our findings corroborate the essential role of Treg-derived exosomes in modulating the inflammatory response and preserving the functional homeostasis of the intestinal epithelium, aligning with our prior research.[8] Nonetheless, our investigation revealed that Treg exosomes do not seem to directly eliminate ROS accumulated in intestinal epithelial cells and tissues, suggesting a promising avenue for enhancing their therapeutic efficacy. The overproduction of ROS plays a pivotal role in the pathogenesis of IBD, intensifying tissue damage and contributing to chronic inflammation. Consequently, the development of effective strategies for ROS scavenging and inflammation mitigation is crucial for advancing IBD treatment. While broad-spectrum antioxidants such as vitamin C and N-acetylcysteine (NAC) have been explored for their potential to decrease ROS levels,[25] their clinical utility is often limited by issues of bioavailability and stability, highlighting the necessity for alternative approaches.[26]

In recent years, artificial nanoenzymes have garnered significant attention due to their adjustable catalytic activities, diverse enzymatic functions and enhanced stability. Nanomedicine-based antioxidant therapies have been extensively explored for the treatment of various diseases associated with oxidative damage.[11] nCeO exhibits a high density of oxygen vacancy defects, facilitating rapid valence transitions.[27] This characteristic enables nCeO to effectively scavenge ROS by mimicking the activities of superoxide dismutase and catalase, positioning nCeO as a promising candidate for the amelioration of IBD. In this work, nCeO with remarkably antioxidant properties was synthesized and administrated into IBD models. Despite observing mild therapeutic effects, these did not appear to align with the compound's capacity to scavenge ROS, particularly in in vivo experiments. This discrepancy may be attributed to the size-dependent transport characteristics of the nanoparticles. The small size of nCeO confers a higher surface area-to-volume ratio, enhancing its antioxidant properties. However, it also influences its clearance and internalization efficiency in the bloodstream.[28,29] For nCeO, with a size of less than 6 nm, are more readily filtered by the kidneys and excreted in the urine.[30] Additionally, their small size facilitates transcellular trafficking rather than cellular internalization.[13] In our strategy, nCeO and Treg exosomes synergistically enhance each other's functionalities. The nCeO endows Treg exosomes the ability to scavenge ROS, while the exosomes carrier enhances the anti-inflammatory efficacy and stability of nCeO in vivo. The data in this paper further corroborate the advantages of exo@nCeO in terms of anti-inflammatory, antioxidant and therapeutic effects in IBD.

However, it is important to acknowledge several limitations inherent in this study. Firstly, due to technical constraints, we were unable to monitor the in vivo transport and clearance efficiency of nCeO under varying conditions. Furthermore, ethical considerations precluded the collection of a sufficient quantity of human-derived Treg cells, thereby limiting the precision of our conclusions.

Conclusion

The present study provides novel evidence that nCeO-loaded Treg exosomes have the ability to counteract intestinal epithelial damage and reduce inflammatory responses in IBD by scavenging ROS and inhibiting the NF-κB pathway. These encouraging results provide new insights into the clinical management of IBD patients.

Ethics Statement

The animal study protocol was conducted in compliance with the National Research Council's Guide for the Care and Use of Laboratory Animals and approved by the Institutional Animal Care and Use Committee of Renmin Hospital of Wuhan University (Approval No: 20211106). All datasets in this study were downloaded from the public GEO database, which allows researchers to download and analyse public datasets for scientific purposes. The public data used in this study complied with item 1, 2 and 4 of Article 32 of the Measures for Ethical Review of Life Science and Medical Research Involving Human Subjects dated February 18, 2023, China.Therefore, this study was exempted from ethical approval.

Acknowledgments

This research was funded by the Fundamental Research Funds for the Central Universities (2042024YXA002), the Shenzhen Science and Technology of Program (JCYJ20220530140609019 and JCYJ20230807090205011), the Interdisciplinary Innovative Talents Foundation from Renmin Hospital of Wuhan University (JCRCZN-2022-018).

Disclosure

The authors report no conflicts of interest in this work.

References

1. Peng Y, Zhu J, Li Y, Yue X, Peng Y. Almond polysaccharides inhibit DSS-induced inflammatory response in ulcerative colitis mice through NF-kappaB pathway. *Int J Biol Macromol*. 2024;281(Pt 1):136206. doi:10.1016/j.ijbiomac.2024.136206
2. Ullah H, Deng T, Ali M, et al. Sea conch peptides hydrolysate alleviates DSS-induced colitis in mice through immune modulation and gut microbiota restoration. *Molecules*. 2023;28(19):6849. doi:10.3390/molecules28196849
3. Hiraoka S, Fujiwara A, Toyokawa T, et al. Multicenter survey on mesalamine intolerance in patients with ulcerative colitis. *J Gastroenterol Hepatol*. 2021;36(1):137–143. doi:10.1111/jgh.15138
4. Van NT, Zhang K, Wigmore RM, et al. Dietary L-Tryptophan consumption determines the number of colonic regulatory T cells and susceptibility to colitis via GPR15. *Nat Commun*. 2023;14(1):7363. doi:10.1038/s41467-023-43211-4
5. Boehm F, Martin M, Kesselring R, et al. Deletion of Foxp3+ regulatory T cells in genetically targeted mice supports development of intestinal inflammation. *BMC Gastroenterol*. 2012;12:97. doi:10.1186/1471-230X-12-97
6. Sakaguchi S, Mikami N, Wing JB, Tanaka A, Ichiyama K, Ohkura N. Regulatory T cells and human disease. *Annu Rev Immunol*. 2020;38:541–566. doi:10.1146/annurev-immunol-042718-041717
7. Mathieu M, Martin-Jaular L, Lavieu G, Thery C. Specificities of secretion and uptake of exosomes and other extracellular vesicles for cell-to-cell communication. *Nat Cell Biol*. 2019;21(1):9–17. doi:10.1038/s41556-018-0250-9
8. Liao F, Lu X, Dong W. Exosomes derived from T regulatory cells relieve inflammatory bowel disease by transferring miR-195a-3p. *IUBMB Life*. 2020. doi:10.1002/iub.2385
9. Hwang J, Jin J, Jeon S, et al. SOD1 suppresses pro-inflammatory immune responses by protecting against oxidative stress in colitis. *Redox Biol*. 2020;37:101760. doi:10.1016/j.redox.2020.101760
10. Tian T, Wang Z, Zhang J. Pathomechanisms of oxidative stress in inflammatory bowel disease and potential antioxidant therapies. *Oxid Med Cell Longev*. 2017;2017:4535194. doi:10.1155/2017/4535194
11. Zhang C, Wang H, Yang X, et al. Oral zero-valent-molybdenum nanodots for inflammatory bowel disease therapy. *Sci Adv*. 2022;8(37):eabp9882. doi:10.1126/sciadv.abp9882
12. Ren X, Zhuang H, Zhang Y, Zhou P. Cerium oxide nanoparticles-carrying human umbilical cord mesenchymal stem cells counteract oxidative damage and facilitate tendon regeneration. *J Nanobiotechnology*. 2023;21(1):359. doi:10.1186/s12951-023-02125-5
13. Xu M, Qi Y, Liu G, Song Y, Jiang X, Du B. Size-dependent in vivo transport of nanoparticles: implications for delivery, targeting, and clearance. *ACS Nano*. 2023;17(21):20825–20849. doi:10.1021/acsnano.3c05853
14. Tenchov R, Bird R, Curtze AE, Zhou Q. Lipid nanoparticles horizontal line from liposomes to mRNA vaccine delivery, a landscape of research diversity and advancement. *ACS Nano*. 2021;15(11):16982–17015. doi:10.1021/acsnano.1c04996
15. Kooijmans SA, Vader P, van Dommelen SM, van Solinge WW, Schiffelers RM. Exosome mimetics: a novel class of drug delivery systems. *Int J Nanomedicine*. 2012;7:1525–1541. doi:10.2147/IJN.S29661
16. Mondal J, Pillarisetti S, Junnuthula V, et al. Hybrid exosomes, exosome-like nanovesicles and engineered exosomes for therapeutic applications. *J Control Release*. 2023;353:1127–1149. doi:10.1016/j.jconrel.2022.12.027
17. Qin YT, Zhao RF, Qin H, et al. Colonic mucus-accumulating tungsten oxide nanoparticles improve the colitis therapy by targeting Enterobacteriaceae. *Nano Today*. 2021;39:101234.
18. Shao M, Yan Y, Zhu F, et al. Artemisinin analog SM934 alleviates epithelial barrier dysfunction via inhibiting apoptosis and caspase-1-mediated pyroptosis in experimental colitis. *Front Pharmacol*. 2022;13:849014. doi:10.3389/fphar.2022.849014
19. Tang K, Kong D, Peng Y, et al. Ginsenoside Rc attenuates DSS-induced ulcerative colitis, intestinal inflammatory, and barrier function by activating the farnesoid X receptor. *Front Pharmacol*. 2022;13:1000444. doi:10.3389/fphar.2022.1000444
20. Wallace KL, Zheng LB, Kanazawa Y, Shih DQ. Immunopathology of inflammatory bowel disease. *World J Gastroenterol*. 2014;20(1):6–21. doi:10.3748/wjg.v20.i1.6

21. Friedrich M, Pohin M, Powrie F. Cytokine networks in the pathophysiology of inflammatory bowel disease. *Immunity*. 2019;50(4):992–1006. doi:10.1016/j.immuni.2019.03.017
22. Gomez-Bris R, Saez A, Herrero-Fernandez B, Rius C, Sanchez-Martinez H, Gonzalez-Granado JM. CD4 T-cell subsets and the pathophysiology of inflammatory bowel disease. *Int J mol Sci*. 2023;24(3):2696.
23. Acharya S, Timilshina M, Jiang L, et al. Amelioration of experimental autoimmune encephalomyelitis and DSS induced colitis by NTG-A-009 through the inhibition of Th1 and Th17 cells differentiation. *Sci Rep*. 2018;8(1):7799. doi:10.1038/s41598-018-26088-y
24. Hang S, Paik D, Yao L, et al. Bile acid metabolites control T(H)17 and T(reg) cell differentiation. *Nature*. 2019;576(7785):143–148. doi:10.1038/s41586-019-1785-z
25. Maestro C, Leache L, Gutierrez-Valencia M, et al. Efficacy and safety of N-acetylcysteine for preventing post-intravenous contrast acute kidney injury in patients with kidney impairment: a systematic review and meta-analysis. *Eur Radiol*. 2023;33(9):6569–6581. doi:10.1007/s00330-023-09577-1
26. Rushworth GF, Megson IL. Existing and potential therapeutic uses for N-acetylcysteine: the need for conversion to intracellular glutathione for antioxidant benefits. *Pharmacol Ther*. 2014;141(2):150–159. doi:10.1016/j.pharmthera.2013.09.006
27. Das S, Dowding JM, Klump KE, McGinnis JF, Self W, Seal S. Cerium oxide nanoparticles: applications and prospects in nanomedicine. *Nanomedicine*. 2013;8(9):1483–1508. doi:10.2217/nnm.13.133
28. Celardo I, Pedersen JZ, Traversa E, Ghibelli L. Pharmacological potential of cerium oxide nanoparticles. *Nanoscale*. 2011;3(4):1411–1420. doi:10.1039/c0nr00875c
29. Kumar A, Hung CH, Hsieh SL, et al. Makoplasty medial unicondylar knee replacement: correction or postoperative angle matters? *Int J Med Robot*. 2022;18(2):e2356. doi:10.1002/rcs.2356
30. Sindhwani S, Syed AM, Ngai J, et al. The entry of nanoparticles into solid tumours. *Nat Mater*. 2020;19(5):566–575. doi:10.1038/s41563-019-0566-2